Scanning Microscopy

Volume 2 | Number 2 Article 50

2-6-1988

Calcium Pyrophosphate Crystal Deposition: The Effect of Soluble Iron in a Kinetic Study Using a Gelatin Matrix Model

Gretchen S. Mandel
Medical College of Wisconsin

Paul B. Halverson
Clement J. Zablocki VA Medical Center

Neil S. Mandel
St. Luke's Hospital

Scanning Microscopy, Vol. 2, No. 2, 1988 (Pages 1177-1188)
Scanning Microscopy International, Chicago (AMF O'Hare), IL 60666 USA

CALCIUM PYROPHOSPHATE CRYSTAL DEPOSITION: THE EFFECT OF SOLUBLE IRON IN A KINETIC STUDY USING A GELATIN MATRIX MODEL

Gretchen S. Mandel*, Paul B. Halverson, and Neil S. Mandel

Department of Medicine, Rheumatology Section,
Medical College of Wisconsin,
Research Service, Clement J. Zablocki VA Medical Center,
and St. Luke's Hospital, Milwaukee, Wisconsin.

(Received for publication May 08, 1987, and in revised form February 06, 1988)

Abstract

The kinetics of calcium pyrophosphate dihydrate (CPPD) crystal growth was studied by allowing calcium and pyrophosphate (PPi^{-4}) ions to diffuse through a denatured collagen matrix (biological grade gelatin) in the presence of either ferric or ferrous ions. Ferric and, to some extent, ferrous ions blocked the migration of the PPi^{-4} diffusion gradient. This retardation in the [PPi^{-4}] gradient led to numerous changes in the patterns of CPPD crystal formation. At the initial stages of crystal growth, the iron ions induced more crystal growth compared to control. At later incubation times, ferrous and ferric ions enhanced crystal growth at the expense of crystal nucleation. The presence of both ferrous and ferric ions resulted in the more rapid formation of the two crystals observed *in vivo*, triclinic CPPD and monoclinic CPPD. Further, both ferrous and ferric ions also reduced the solubility of the crystalline material in the broad diffuse band which formed when the Ca^{+2} and PPi^{-4} gradients first met. In this system, the presence of either ferrous or ferric ions increased the amount of hydroxyproline included in the crystalline precipitates. Iron was also incorporated into the crystals, particularly into the triclinic CPPD and monoclinic CPPD crystals.

Key words: Calcium pyrophosphate, Chondrocalcinosis, Pseudogout, Crystals, Crystallization, Kinetics, Gelatin matrix, Model system, Ferrous ions, Ferric ions

*Address for correspondence:
Gretchen S. Mandel
Research Service/151
The Clement J. Zablocki VA Medical Center
Milwaukee, WI 53295
Phone number 414-384-2000 ext. 2498

Introduction

There is a high probability of an association between calcium pyrophosphate crystal deposition disease and hemochromatosis [18]. Nearly one half of patients with hemochromatosis have arthritis and half of these have radiographic evidence of chondrocalcinosis [4,5,7]. Iron itself may be directly related to the calcific deposits since calcium pyrophosphate crystal deposits have also been observed in patients with transfusion hemosiderosis [1,22]. Chondrocalcinosis also occurs in patients with hemophilia [10,12]. Pediatric exposure to iron seems to enhance its deleterious effects as evidenced by the more frequent occurrence of calcium pyrophosphate crystal deposition in hemochromatosis than in other iron overload syndromes [9,21]. Also, experimental iron loading of rabbits induced cartilage degeneration only when initiated early in life [2].

In ultrastuctural studies of synovial membranes in hemochromatosis, hemosiderin deposits were seen in each type of lining cell, but were most common in the Type B cells which are rich in rough endoplasmic reticulum [19]. Iron aggregrates were observed to be either membrane bound or free in the cytoplasm. However, calcium pyrophosphate dihydrate (CPPD) crystalline deposits were not located near either the ferritin or the hemosiderin particles. In a similar study on articular cartilage [20], iron was located within chondrocytes, and both apatite and CPPD crystals were identified in locations other than those proximal to ferritin particles.

It is not clear how tissue bound iron affects the formation of CPPD crystals. *In vitro* studies have indicated that ferrous, but not ferric, ions inhibit some inorganic pyrophosphatases [16]. In an *in vitro* solution crystal growth study, ferric ions were shown to promote CPPD crystal growth at lower pyrophosphate (PPi^{-4}) levels [8]. Studies in rabbits have shown that synovial hemosiderosis slows the metabolic clearance of radiolabelled CPPD crystals from joints by about 50% [17].

We have previously reported using calcium (Ca^{+2}) and PPi^{-4} ionic diffusion through a denatured collagen (biological grade gelatin) matrix to induce CPPD crystal growth as a reproducible *in vitro* model system for CPPD deposition in cartilage [13-15]. We now report the use of this model system to study the effect of soluble iron on Ca^{+2} and PPi^{-4} ionic diffusion and on CPPD crystal nucleation and growth.

Materials and Methods

Gel Preparation

Gels were prepared as described previously [13]. Briefly, all glassware was washed, soaked in bleach for 24 h, thoroughly rinsed in doubly-distilled water, and siliconized with an organo-silicone surfactant (Masil-1066-D, Maser Chemicals, Gurnee, IL). Gelatin solutions (5% w/v) were prepared using biological grade gelatin, Bloom #275, (Fisher Scientific, Chicago, IL). Eighty percent of the dry weight of the gelatin was estimated to be collagen based on its hydroxyproline content [23]. The remaining 20% was determined to be a mixture of unidentified proteins and small peptides. The gelatin was found to contain only type I collagen by sodium dodecyl sulfate gel electrophoresis [3]. The commercially available gelatin is derived from porcine skin and contains all physiologic ions at approximately 25-30% of their normal concentrations. The base levels of Ca^{+2} = 0.5 mM, Mg^{+} = 0.1 mM, PO_4 = 0.3 mM, and PPi^{-4} < 0.01 mM in the 5% gelatin solution were determined by atomic absorption and spectrophotometric assays as detailed below.

Study I. The effect of excess calcium ions as a control

This study was previously published [13], but serves as one of the controls for the current study, and is therefore repeated here. Gels were poured in 20 identical 200 x 22 mm test tubes in four equal partitions of 15 ml each. The lowest partition contained gelatin and 10 mM sodium pyrophosphate (Fisher Chemical Co, Chicago, IL), the middle two partitions (one-half of the total volume) contained gelatin alone, and the upper partition contained gelatin and 50 mM calcium acetate (Fisher Chemical Co, Chicago, IL). Each partition was prepared immediately before use, adjusted to pH = 7.0 with either NaOH or acetic acid, layered separately into the test tubes while hot, and then cooled in an ice bath. The length of the ion free band was 8 cm. Sodium azide, 0.3 M, was added to all solutions since fungal growth occurred if the azide concentration was below 0.25 M. This had no effect on crystal growth.

The tubes were allowed to incubate for predetermined times at 23° C; the gels melted above 30° C. Duplicate tubes (which were morphologically identical in all cases) were harvested at weeks 1, 2, 3, 4, 5, 6, 7, 8, 10, and 12 by removing the entire gelatin cylinder intact from the test tube. Each cylinder was sliced into 8 layers, each being 2 cm long, and the crystals removed as described below. Crystals grew in the lower 5 layers which were pooled from the duplicate tubes and saved for further analysis.

Study II. The effect of ferric ions with excess calcium ions

Gels were prepared as described for Study I, with the exception that five partitions were poured. The lowest partition was 15 ml of gelatin plus 10 mM pyrophosphate, the next partition was 5 ml of ion-free gelatin, the next was 20 ml of gelatin plus 0.5 mM $FeCl_3$, followed by another 5 ml of ion-free gelatin, and finally 15 ml of 50 mM calcium acetate. Gel tubes were harvested as described for Study I.

Study III. The effect of excess pyrophosphate ions as a control

This study was also previously published [13], but serves as one of the controls for the current study, and is therefore repeated here. Gels were poured in 15 identical 100 x 11 mm test tubes in four equal partitions of 2.5 ml each. The lowest partition contained 50 mM sodium pyrophosphate, the middle two partitions were again ion-free, and the upper partition contained 50 mM $CaCl_2$. All solutions were prepared as described above except that they contained 0.4 M sodium azide. The length of the ion-free zone was 4.0 cm.

The gel tubes were harvested on days 4, 6, 7, 10, 12, 14, 19, 26, 33, 40, 47, 55, 69, 97, 125, and 153. The entire gelatin cylinder was removed as described above, sliced into 7 equal layers which were saved for further analysis.

Studies IV and V. The effect of ferric and ferrous ions in the presence of excess pyrophosphate ions

Gels were prepared as described for Study III, with the exception that five partitions were poured. The lowest partition was 2.5 ml of gelatin plus 50 mM pyrophosphate, the next partition was 2.0 ml of ion-free gelatin, the next was 1.0 ml gelatin plus 0.02 mM $FeCl_3$ for Study IV and 0.02 mM $FeCl_2$ for Study V, followed by another 2.0 ml of ion-free gelatin, and finally 2.5 ml of gelatin plus 50 mM $CaCl_2$. The gel tubes were harvested as described in Study III.

Crystal Characterization

For all studies, the gelatin layers were melted at 50°C, the final pH checked, and the crystalline material isolated by centrifugation, washed twice with 1 ml of warm doubly distilled water, and air-dried. All samples were characterized with high resolution X-ray powder diffraction using copper radiation at 15 mA and 45 kV using an XRD-5 generator (General Electric, Milwaukee, WI). Samples containing sufficient material were mounted on aluminum foil (Reynolds Wrap, Richmond, VA) for internal diffraction standardization and diffracted using a quartz crystal monochromated Guinier diffraction camera (Huber Instruments, Rimsting, West Germany). Samples containing little material were mounted on Magic Transparent Tape (3M, Minneapolis, MN) and diffracted for 20 h using a quartz crystal monochromated Guinier camera (Philips Electronic Instruments, Mahwah, NJ). For these samples, the image of the primary X-ray beam was used to standardize the diffraction maximum. Diffraction patterns were either measured or compared to those of known pyrophosphate structures [11]. The term amorphous was used if there was a significant amount of precipitate, yet no diffraction pattern was obtained. If a small amount of precipitate was observed with no diffraction pattern, the material was labeled unknown. It is possible that some of the material assigned "U" may in fact be amorphous.

Representative samples were mounted on planchets, coated with carbon, and were characterized with scanning electron microscopy (Model 1200, Advanced Metals Research Corporation, Bedford, MA). The calcium:phosphorus and iron:phosphorus ratios were determined using an energy dispersive analyzer (EEDSII EG and G Ortec, Oak Ridge, IL).

Pyrophosphate Concentration Determination.

The pyrophosphate concentration was determined by a modification of the method of Fiske and SubbaRow [6] using test kits (Sigma Chemical Company, St. Louis, MO). An aliquot of each gel section (0.25 ml) was incubated with 5.0 ml of 1.0 N HCl for 24 h to solubilize the gelatin and hydrolyze the pyrophosphate ions. It was necessary to use HCl in place of trichloroacetic acid in the gelatin system since it induced protein precipitation which scavenged both phosphate and pyrophosphate ions. Optical absorbance was determined at 660 nm on a Model 250 Spectrophotometer (Gilford Instruments, Oberlin, OH) and concentrations determined against known standards prepared in the presence of gelatin. Assays were done in triplicate with an average standard error of 0.005 mM.

Calcium and Iron Concentration Determinations

Calcium ion concentration was determined by atomic absorption analysis (Model AA-1475ABD, Varian Associates, Palo Alto, CA). A 0.30 ml aliquot of gel was diluted with a solution containing 1 % $LaCl_3$ in 5% HCl according to standard procedures. Concentrations were

determined with a 1000 microgram/ml [Ca^{+2}] standard in 2% HCl (Aldrich Chemical, Milwaukee, WI) diluted as above. Determinations were done in triplicate; the average standard error was 0.05 mM. The magnesium concentration in the gel and the iron concentrations for Study II were determined using similar, standard techniques.

Preparation of Ion Gradient Contour Plots

The [Ca^{+2}] was plotted as a function of tube position and time and then the plot was contoured. The [PPi^{-4}] contour plot was constructed in the same manner and the two plots superimposed photographically. The crystals which had been identified at each tube position and time point were then added to the composite ionic gradient plots. The iron contour plot for Study II was constructed in a similar manner.

Determination of Hydroxyproline Inside Crystalline Samples

One ml of 1 N HCl was added to selected samples of crystalline precipitates. This dissolved a portion of all of the samples, however for the early (4 to approximately 7 days) samples, a fine net of material remained which was dissolved three days later after the addition of 0.5 ml of 5 N HCl. The pH of the solution was returned to 7 with NaOH. The total hydroxyproline concentration was then determined spectrophotometrically following standard procedures [23]. The hydroxyproline concentration was determined singly on the entire sample due to its small size.

Computer Sorts

Each slice with its associated tube position, time, [Ca^{+2}], [PPi^{-4}], pH, and crystal type was entered into a data file. The data file was sorted according to these variables by the program CORLATE written by the authors for an Eclipse S/230 (Data General, Boston, MA). The program allows for nested sorts of up to 10 variables as well as for sorts holding up to 10 variables constant at input values. This program was used to determine the maximum and minimum [Ca^{+2}], [PPi^{-4}], and ion products associated with each crystal type.

Results

The diffusion of Ca^{+2} and PPi^{-4} ions through the matrix environment provided by the biological gelatin leads to the formation of various crystallographic forms of calcium pyrophosphate crystals. These calcium pyrophosphate dimorphs nucleate, grow, dissolve, and transform over time. The experimental design has allowed for the kinetic analysis of these crystallization processes. The model system has yielded the *in vivo* crystals, triclinic calcium pyrophosphate dihydrate (t-CPPD) and monoclinic (m-CPPD). In addition, the system has produced crystals of orthorhombic calcium pyrophosphate tetrahydrate (o-CPPT), two mixed Ca^{+2}/Na^{+} pyrophosphate salts, and amorphous calcium pyrophosphate. The crystal types will be denoted t-CPPD (t), m-CPPD (m), o-CPPT (o), C, D, and a, respectively; the nomenclature N indicates no crystal growth, and U indicates insufficient crystalline material which could not be identified using X-ray diffraction.

The kinetics of the crystal growth process have been analyzed using ionic gradient maps of the changes in [Ca^{+2}] and [PPi^{-4}] as a function of time of incubation, of the crystal type formed, and of the specific position within the tube (Figures 1-6). The maximum and minimum [Ca^{+2}] and [PPi^{-4}], ion product, and time of formation for the various crystal types are shown for Studies I, II, III, IV, and V in Table 1.

Study I

As shown in Figure 1, the control with excess of

Figure 1:. The kinetics of CPPD crystal growth in the presence of excess Ca^{+2} (Study I, control for Study II). Both the [Ca^{+2}] and [PPi^{-4}] have been contoured at 1 mM increments, using dashed lines for [Ca^{+2}], and solid lines for [PPi^{-4}]. No contours are included for concentrations in excess of 10 mM for clarity. Only the lower 10 cm of gel are shown since no crystals formed in the upper, Ca^{+2} rich layers.

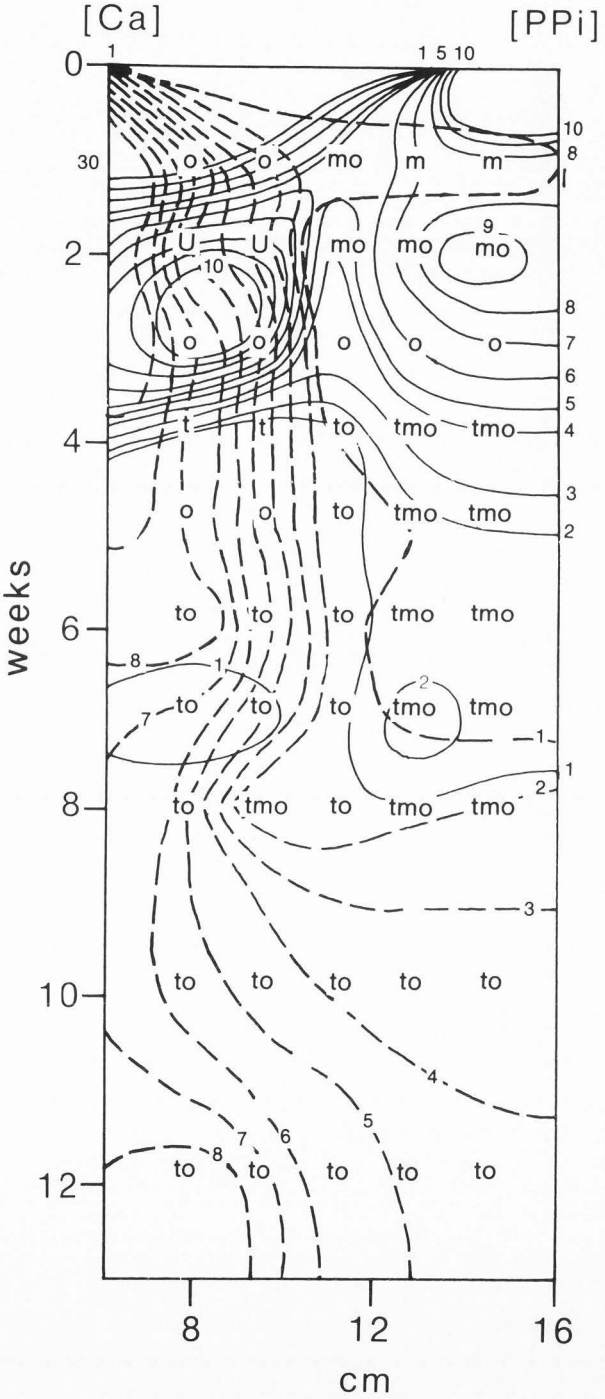

Table 1: Minimum and maximum [Ca^{+2}], [PPi^{-4}], ion product, and time of formation for the various crystal types along with the total number and frequency of occurrence as a percentage of the total number of observations. The overall minimum and maximum values for each study are presented as "total". The ion product is expressed as [Ca^{+2}]^2 * [PPi^{-4}], since the chemical formula for CPPD is $Ca_2P_2O_7$. ND indicates not determined.

	#	%	[Ca^{+2}] mM	[PPi^{-4}] mM	[Ca^{+2}]^2*[PPi^{-4}] M_3	TIME days
STUDY I	**(Control, Excess Ca^{+2}, no added Fe)**					
t	33	41	0.2 - 8.2	0.0 - 4.1	2.0×10^{-11} - 1.1×10^{-7}	28 - 84
m	17	21	0.2 - 8.0	0.0 - 9.1	3.0×10^{-11} - 1.0×10^{-8}	7 - 84
o	44	55	0.2 - 8.2	0.0 - 10.2	2.0×10^{-11} - 6.5×10^{-7}	7 - 84
a	2	3	5.7 - 5.7	9.2 - 9.2	3.0×10^{-7} - 3.0×10^{-7}	14 - 14
N	30	38	ND	ND	ND	7 - 84
total	80		0.3 - 8.20	0.0 - 10.2	2.0×10^{-11} - 6.5×10^{-7}	7 - 84
STUDY II	**(Excess Ca^{+2}, $FeCl_3$)**					
t	11	14	4.7 - 10.6	0.0 - 3.2	9.0×10^{-11} - 6.1×10^{-8}	14 - 84
m	15	19	0.6 - 8.7	0.2 - 8.3	2.1×10^{-9} - 6.1×10^{-8}	7 - 84
o	33	41	0.6 - 9.7	0.0 - 8.3	9.0×10^{-11} - 6.1×10^{-8}	7 - 84
u	4	5	0.5 - 9.1	1.6 - 5.2	6.5×10^{-8} - 1.3×10^{-7}	21 - 28
N	33	41	ND	ND	ND	7 - 84
total	80		0.5 - 10.6	0.0 - 8.3	9.0×10^{-11} - 1.3×10^{-7}	7 - 84
STUDY III	**(Control, Excess PPi^{-4}, no added Fe)**					
t	3	3	0.2 - 0.2	2.7 - 5.5	1.1×10^{-10} - 2.2×10^{-10}	97 - 125
m	25	22	0.1 - 2.1	2.0 - 8.7	5.0×10^{-11} - 8.8×10^{-9}	26 - 153
o	51	46	0.1 - 7.1	0.0 - 9.3	5.0×10^{-11} - 3.9×10^{-8}	4 - 153
a	5	4	8.2 - 16.0	0.0 - 2.0	2.3×10^{-10} - 1.3×10^{-7}	4 - 12
u	3	3	0.3 - 0.5	4.6 - 13.3	6.1×10^{-10} - 2.1×10^{-9}	14 - 40
N	29	44	0.1 - 31.7	0.0 - 30.7	1.0×10^{-11} - 2.9×10^{-7}	1 - 153
C	11	2	0.2 - 0.8	4.0 - 25.8	1.6×10^{-10} - 2.8×10^{-9}	4 - 153
D	23	5	0.2 - 0.8	1.5 - 29.9	1.1×10^{-10} - 1.1×10^{-8}	4 - 153
total	112		0.1 - 31.7	0.0 - 30.7	1.0×10^{-11} - 1.3×10^{-7}	1 - 153
STUDY IV	**(Excess PPi^{-4}, $FeCl_3$)**					
t	7	6	0.1 - 3.6	0.0 - 4.5	3.0×10^{-11} - 7.0×10^{-10}	19 - 125
m	19	17	0.1 - 7.2	0.0 - 4.7	1.0×10^{-11} - 4.1×10^{-9}	10 - 153
o	51	46	0.1 - 7.2	0.0 - 5.8	1.0×10^{-11} - 1.8×10^{-8}	4 - 153
a	6	5	0.2 - 14.8	0.0 - 29.2	1.9×10^{-10} - 7.3×10^{-9}	4 - 40
u	6	5	0.1 - 0.2	1.4 - 6.0	2.0×10^{-11} - 2.4×10^{-10}	26 - 153
N	33	21	0.1 - 30.8	0.0 - 44.8	2.0×10^{-11} - 6.1×10^{-8}	4 - 153
C	6	4	0.1 - 0.4	4.0 - 30.3	4.0×10^{-11} - 2.7×10^{-9}	4 - 125
D	14	9	0.1 - 0.5	0.6 - 16.8	1.0×10^{-11} - 1.0×10^{-9}	4 - 153
total	112		0.1 - 30.8	0.0 - 44.8	1.0×10^{-11} - 6.1×10^{-8}	4 - 153
STUDY V	**(Excess PPi^{-4}, $FeCl_2$)**					
t	13	12	0.1 - 0.6	3.1 - 6.2	4.0×10^{-11} - 1.4×10^{-9}	33 - 153
m	24	21	0.1 - 4.0	0.0 - 8.3	2.0×10^{-11} - 3.2×10^{-9}	19 - 153
o	55	49	0.1 - 8.2	0.0 - 26.0	4.0×10^{-11} - 9.1×10^{-9}	4 - 153
a	7	6	0.2 - 20.9	0.0 - 23.4	9.4×10^{-10} - 2.3×10^{-7}	4 - 12
u	4	4	0.1 - 0.4	4.8 - 28.6	5.0×10^{-11} - 2.6×10^{-8}	7 - 125
N	33	29	0.1 - 28.9	0.0 - 34.9	5.0×10^{-11} - 5.1×10^{-7}	4 - 153
C	12	11	0.1 - 0.4	0.3 - 16.4	1.0×10^{-11} - 1.5×10^{-9}	10 - 153
D	16	14	0.1 - 0.5	1.5 - 26.0	6.0×10^{-11} - 2.3×10^{-9}	4 - 153
total	112		0.1 - 28.9	0.0 - 34.9	5.0×10^{-11} - 5.1×10^{-7}	4 - 153

Ca^{+2}, the variation in the calcium concentration has been contoured in 1 mM increments using dashed lines originating from the upper left of the plot (the top of the growth tube), and the PPi^{-4} concentrations have been contoured in 1 mM increments in solid lines originating from the right of the plot (the bottom of the tube). The contour levels for both ions were omitted when concentrations exceeded 10 mM. Only the lower 10 cm of gel are shown here since no crystals formed in the original calcium doped partition.

The Ca^{+2} and PPi^{-4} gradients migrate to the center of the tube within one week, interact at $[Ca^{+2}]$ = 3-7 mM and $[PPi^{-4}]$ = 0.5-2 mM with the formation of crystal o-CPPT. Simultaneously, crystals of m-CPPD also formed in the PPi^{-4} rich partitions. Crystal o-CPPT rapidly dissolved at two weeks with a commensurate burst of available PPi^{-4}. Amorphous calcium pyrophosphate formed at 2 weeks at the high $[Ca^{+2}]$ and $[PPi^{-4}]$ and converted to t-CPPD and o-CPPT at 3-4 weeks. At 8 weeks when the ion concentrations had approached physiologic levels, the crystal types included t-CPPD, m-CPPD, and o-CPPT. From Table 1, the ion product varies over 4 orders of magnitude for the various crystals, except for amorphous. The range of ion products and maximum and minimum $[Ca^{+2}]$ and $[PPi^{-4}]$ for crystals t-CPPD, m-CPPD, and o-CPPT were nearly identical.

Study II

As shown in Figure 2, the addition of ferric ions in the presence of excess calcium markedly alters the $[PPi^{-4}]$ gradient. Levels of 1 mM PPi^{-4} were not detectable within the ferric doped layers throughout the 12 weeks of the study. The $[Ca^{+2}]$ gradient remains virtually identical to that observed in Study I with some very small and probably not meaningful alterations. Crystal growth was also markedly affected by the presence of ferric ions. Although m-CPPD formed at 1 week in both the control (Study I) and in the ferric study, the position of crystal formation was different. In the control, m-CPPD crystals formed at 1 week in areas of the gel where $[PPi^{-4}]$ was 5 times greater than $[Ca^{+2}]$. In the ferric study, m-CPPD crystals not only formed in areas of excess of PPi^{-4}, but they also formed in the ferric doped layers where the Ca^{+2} ion concentration was approximately 8 mM and the PPi^{-4} levels were less than 0.01 mM. By week 2, t-CPPD crystals had also appeared in the ferric doped layers, whereas in the control, the first appearance of t-CPPD crystal was week 4 in areas of excess PPi^{-4}.

Figure 3 shows the change in the $[Fe^{+3}]$ in Study II as a function of time, tube position, and crystal type formed. Contour levels were 0.01 mM and the contours with tick marks indicate boundary regions of decreased $[Fe^{+3}]$. The initial formation of m-CPPD and t-CPPD crystals appears to have scavenged substantial amounts of ferric ion from the gels. When these crystals dissolved at week 4 (compare Figures 2 and 3), there was a release from <0.01 mM to >0.04 mM Fe^{+3}. At week 6, t-CPPD reformed, again scavenging ferric ions. As these crystal dissolved at week 7, and new t-CPPD and m-CPPD reformed at week 8, there was again a release followed by scavenging of ferric ions. From Table 1, t-CPPD formed at 14 days rather than at 28 days in the control. The minimum $[Ca^{+2}]$ for t-CPPD formation was 4.7 mM as opposed to 0.2 mM in the control. This is probably a result of the blockage of the PPi^{-4} gradient by the ferric ions, rather than a significant difference in concentration requirements.

Table 2 details the Ca:P and Fe:P ratios for crystalline samples selected to be as representative as possible over the varied conditions observed in the gel. Clearly, the crystals that grew in the iron doped layers (layers 4 and 5) incorporated iron into their crystalline lattices. The amount of incorporated iron was approximately 0.08% w/w.

Figure 2: The kinetics of crystal growth showing the effect of ferric ions in the presence of excess Ca^{+2} (Study II). The ferric ions were added to the gel layers 4 and 5, which are between 6 - 10 cm. The contours are indicated as described in Figure 1.

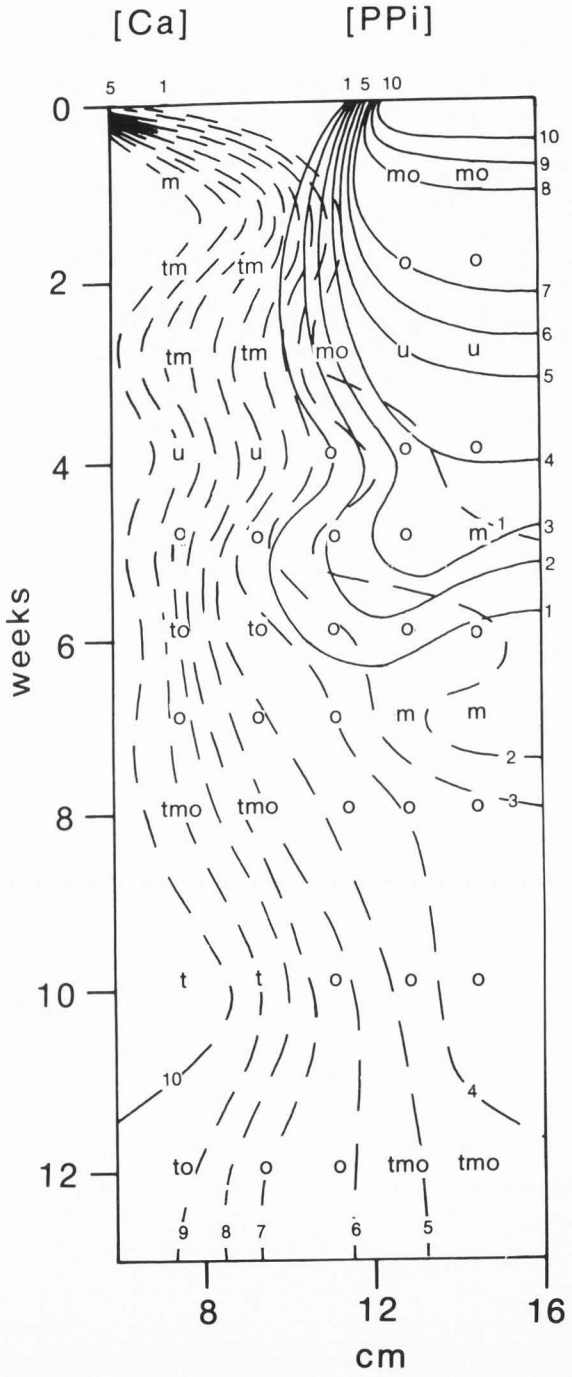

Figure 3: For Study II, a kinetic contour map of the changes in the $[Fe^{+3}]$ as a function of time, tube position, and crystal type formed. Contour levels are 0.01 mM and the contours with tick marks indicate boundary regions leading to decreasing $[Fe^{+3}]$.

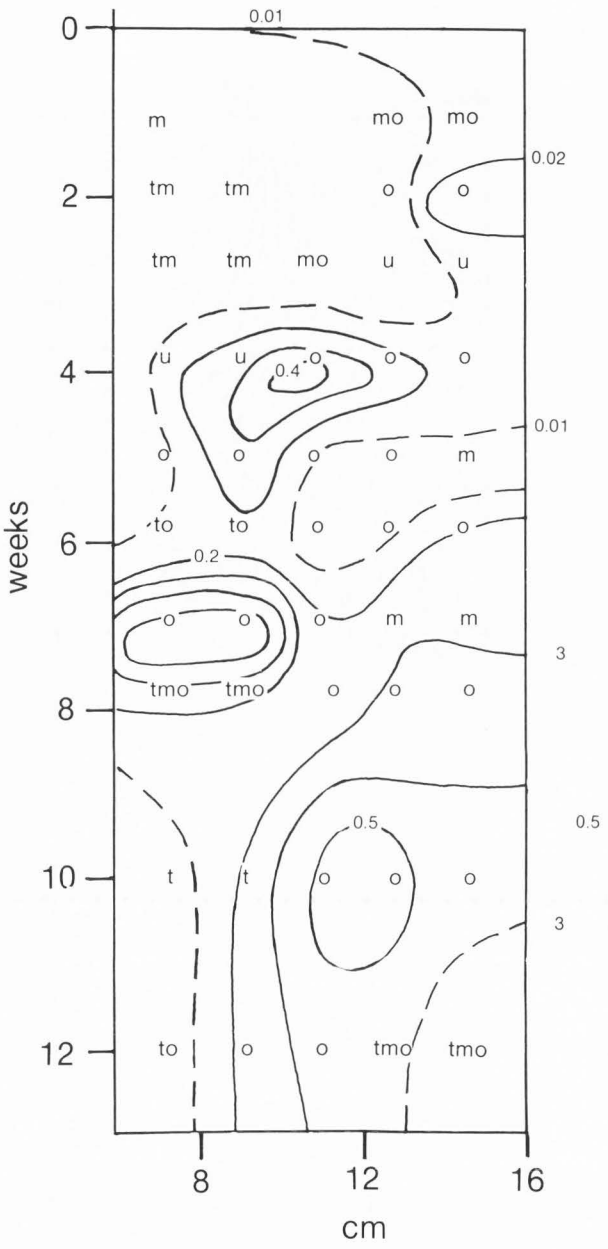

Study III

As shown in Figure 4, the control with excess of PPi^{-4}, the kinetic contour map (Figure 4a) of the ionic gradients indicates that the crystal types formed include t-CPPD, m-CPPD, o-CPPT, a, u, C, and D. Figure 4b shows the photographic progression of crystal formation during the 22 weeks of incubation. At high $[Ca^{+2}]$ and low $[PPi^{-4}]$, amorphous formed, was present for 2 weeks, and then transformed to o-CPPT. O-CPPT crystallized in the center of the tube, forming the milky white band seen in Figure 4b and did not dissolve for 6 weeks. The layers towards the PPi^{-4} rich partition produced the two mixed Ca^{+2}/Na^{+} PPi^{-4} salts which prevailed throughout the study. Of note, is that in contrast to Study I where the ionic gradients had not reached equilibrium by 12 weeks, the excess of PPi^{-4} in Study III appears to have induced ionic equilibrium within the tube at 7 weeks. Also in contrast to Study I, there was relatively little t-CPPD formed in Study III. Further, there was no crystal growth in the PPi^{-4} rich partitions in the bottom of the tubes or in the calcium rich, upper section of the tubes until the $[Ca^{+2}]$ dropped below 10 mM. From Table 1, the range in the ion products for the formation of t-CPPD and m-CPPD is narrower compared to Study I, and there were fewer occurrences of t-CPPD.

Table 2: The Ca:P and Fe:P ratios for selected crystals grown during Study II. Phosphorous is defined as 1. Layers 4 and 5 were doped with ferric ions. Standard deviations are given in parenthesis.

Time (days)	Layer	Ca:P	Fe:P	Crystal
7	4	1.04(0.12)	0.03(0.01)	m
7	7 - 8	1.05(0.11)	0.01(0.01)	mo
35	4 - 5	1.00(0.05)	0.04(0.01)	o
49	4 - 5	1.10(0.09)	0.03(0.01)	o
70	6	0.99(0.07)	0.0	o
84	4	0.92(0.09)	0.04(0.00)	to
84	5	1.11(0.10)	0.0	to

Study IV

As shown in Figure 5, for the effect of ferric ions in the presence of excess PPi^{-4}, the kinetic contour map (Figure 5a) of the ionic gradients indicates that the crystal types formed parallel to those observed in Study III (the control for excess PPi^{-4}, Studies IV and V). Figure 5b shows the photographic progression of crystal formation and dissolution over the 22 weeks of incubation. The first observation in comparison to Figure 4 (the excess PPi^{-4} control) is that the PPi^{-4} ionic gradient did not break through the ferric doped layer until week 3, at which time the $[PPi^{-4}]$ probably reached a level sufficient to bind up all of the ferric ions. At week 2, the $[PPi^{-4}]$ in the PPi^{-4} rich layer dropped to 8 mM, whereas in the control at week 2, the $[PPi^{-4}]$ had only dropped to 20 mM. The amount of crystalline material formed by week 2 in the ferric doped system was significantly greater than in the control. Following week 3 with the PPi^{-4} gradient crossing of the ferric ion barrier, the Ca^{+2} and PPi^{-4} gradients and the crystal types formed are similar between the control and the ferric doped gels. Prior to week 3, the calcium rich layers were deprived of PPi^{-4} as compared to the control, and it is noteworthy that the amorphous materials formed in the control are not common in the ferric doped system. The formation of m-CPPD at day 10 and the formation of t-CPPD at day 19 in the ferric doped system significantly preceded the time of formation in the control (days 26 and 97, respectively). From the photographic composites (Figures 4b and 5b), the addition of ferric ions led to the formation of a broader diffuse band which maintained its structure for 2 additional weeks. Also, following the disappearance of the diffuse band, the ferric doped gel had fewer, yet larger crystalline masses, particularly in the t-CPPD, m-CPPD, and o-CPPT crystal growth sites.

Figure 4: The kinetics of CPPD crystal growth in the presence of excess PPi^{-4} (Study III, control for Studies IV and V). In Figure 4a, the contours are as described in Figure 1, except that both $[Ca^{+2}]$ and $[PPi^{-4}]$ were contoured in 1 mM increments up to 10 mM, above which the increments are 5 mM. The composite photographs monitoring the progressive changes in crystal growth are shown in Figure 4b.

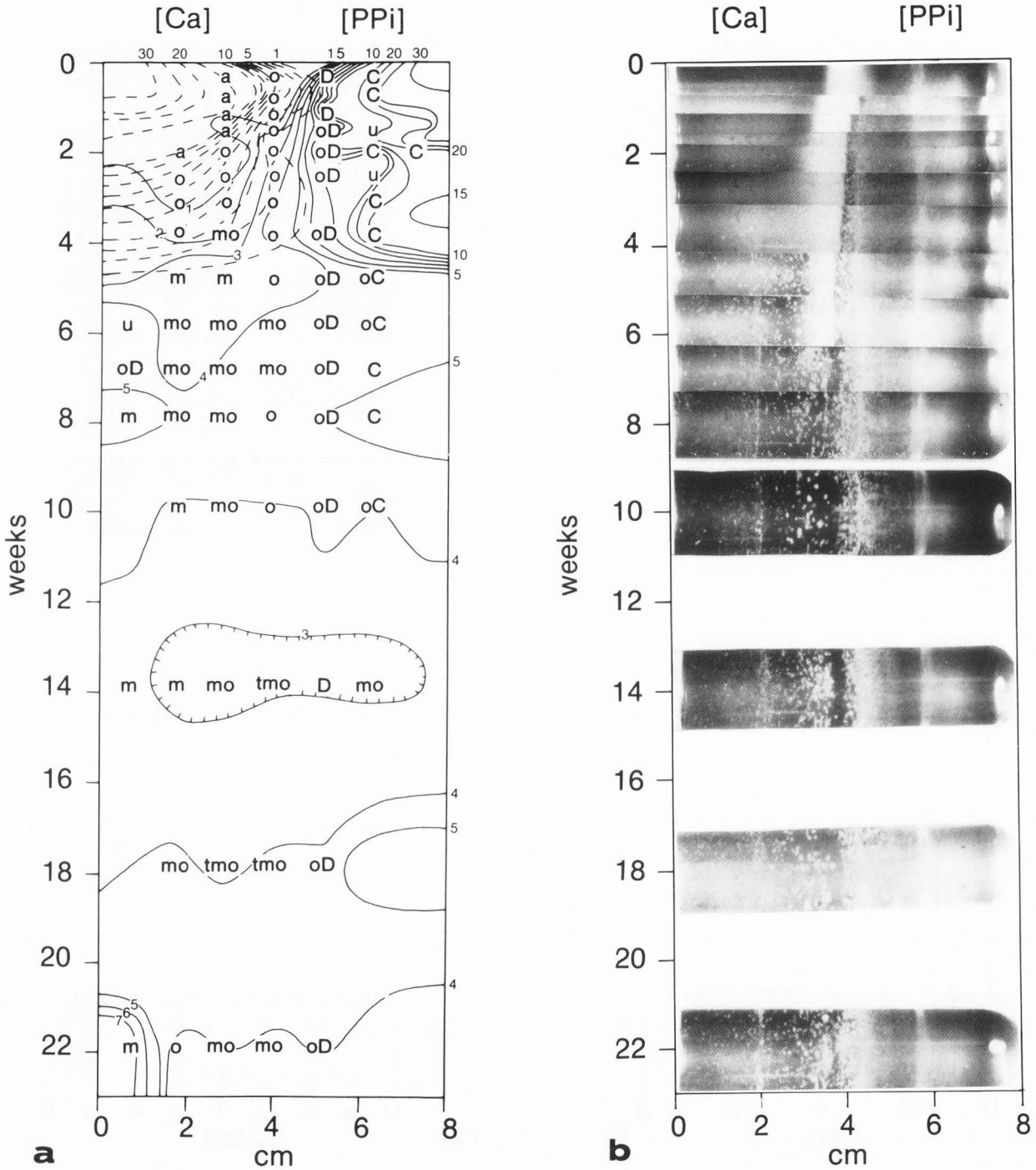

Figure 5: The kinetics of CPPD crystal growth showing the effect of ferric ions in the presence of excess PPi^{-4} (Study IV). In Figure 5a, the contours are as described in Figure 4. The composite photographs monitoring the progressive changes in crystal growth are shown in Figure 5b.

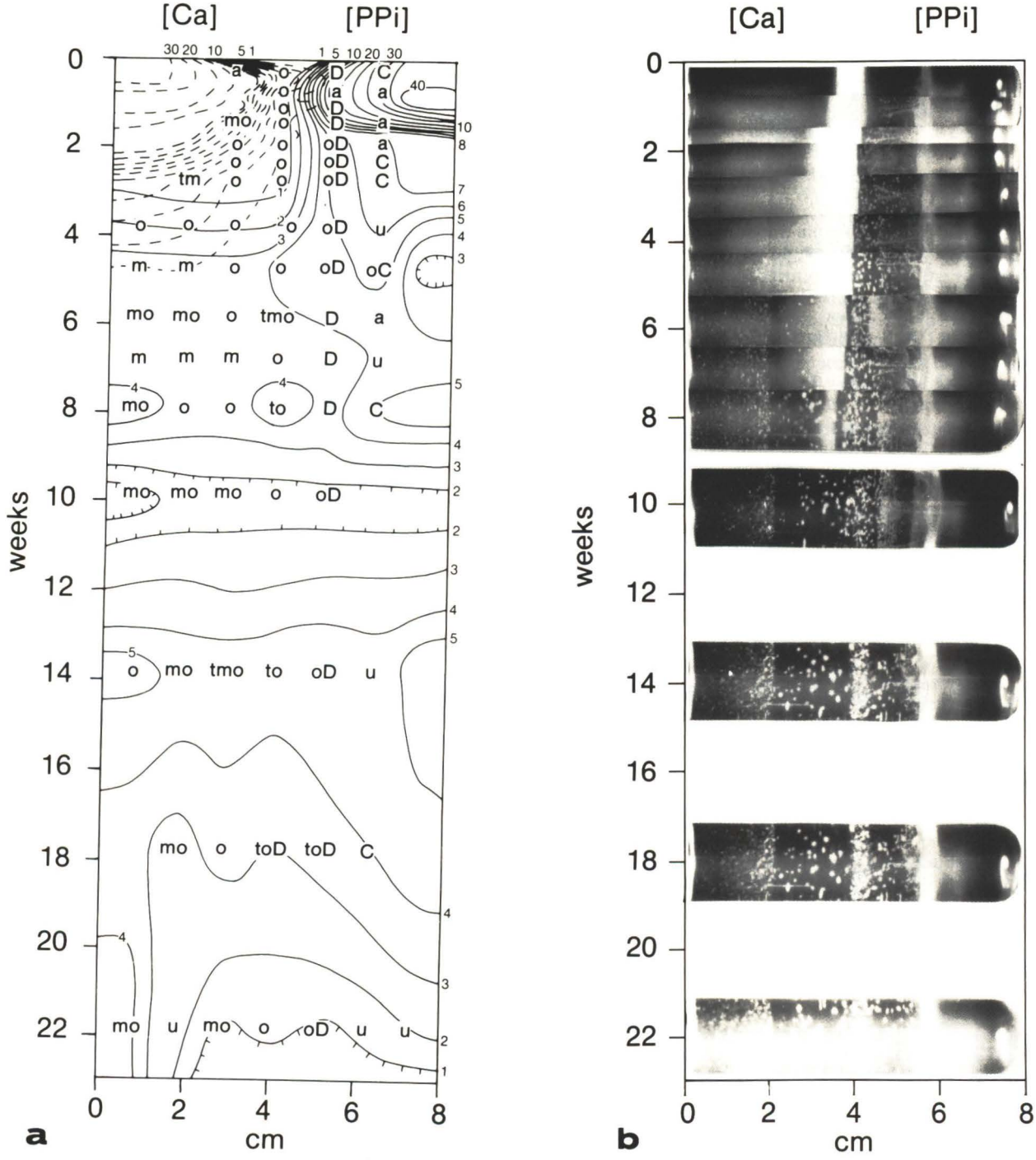

Figure 6: The kinetics of CPPD crystal growth showing the effect of ferrous ions in the presence of excess PPi^{-4} (Study V). In Figure 6a, the contours are as described in Figure 4. The composite photographs monitoring the progressive changes in crystal growth are shown in Figure 6b.

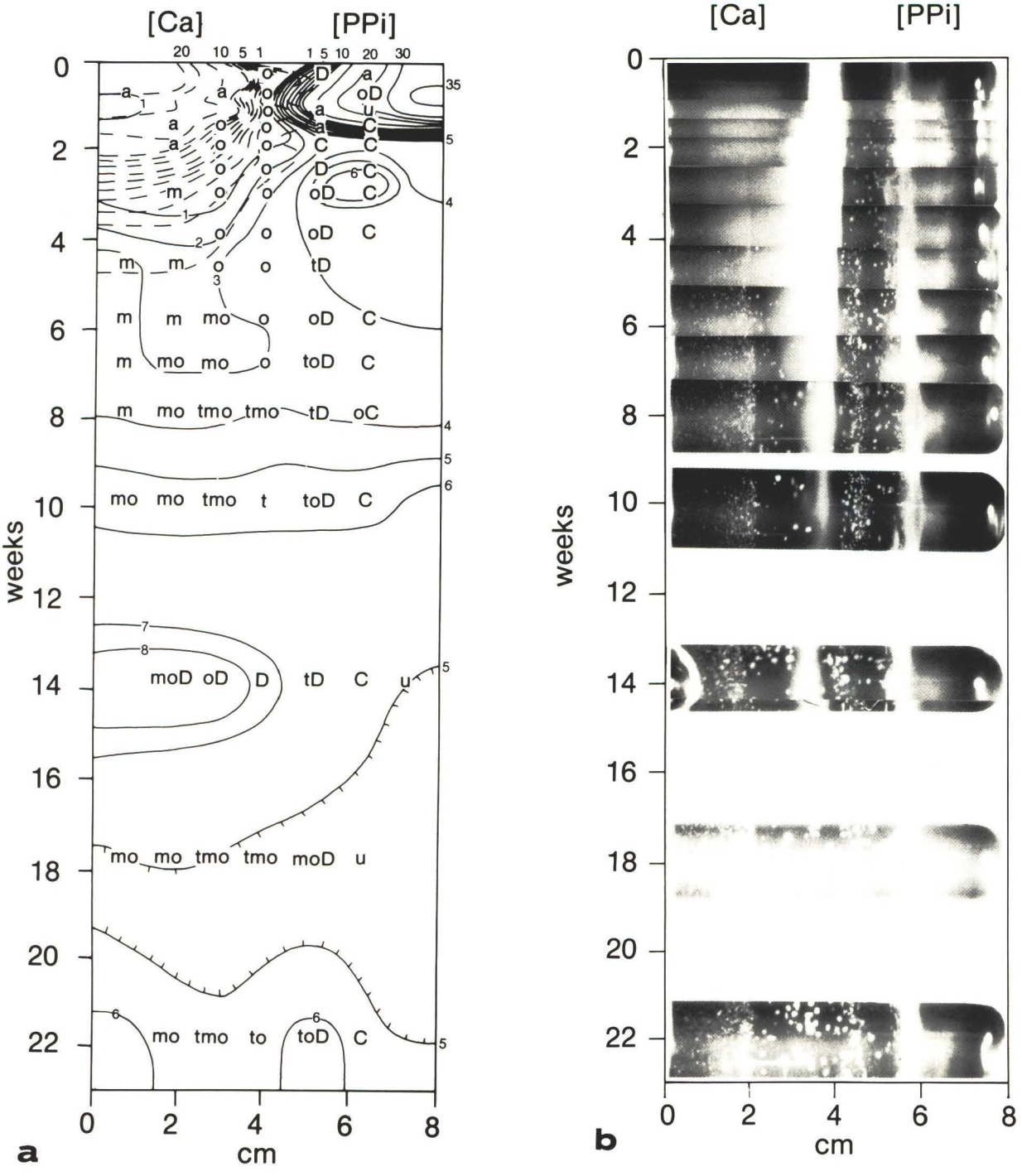

Study V

As shown in Figure 6, the presence of ferrous ions in the presence of excess PPi^{-4}, the kinetic contour map (Figure 6a) indicates that the same crystal types formed as in Studies III and IV. Figure 6b is the photographic composite of the kinetics of crystal formation over the 22 weeks of incubation. The addition of ferrous ions, in comparison to ferric ions, had a less dramatic effect on the migration of the PPi^{-4} gradient. As in Study IV, there was a rapid precipitation of crystalline material at the ferrous ion doped layer as evidenced by the drop in $[PPi^{-4}]$ to 5 mM by week 2. At the third week, some of the crystals which had grown in the PPi^{-4} rich layers dissolved, raising the PPi^{-4} concentration in this region to 6 mM. This released PPi^{-4} then migrated towards the Ca^{+2} gradient. This same influx of fresh PPi^{-4} ions into the PPi^{-4} gradient, which resulted from the dissolution of material deposited in the PPi^{-4} rich layers at early time, was also observed in Study I and, to some extent, Study III. At the end of the study, there is more remaining PPi^{-4} in the ferrous study (5-6 mM) compared to the ferric study (1-4 mM). The diffuse central band which formed in the ferrous ion layer remained longer in the ferrous study than in the ferric Study IV (week 14 compared to week 8, respectively). In general, there are fewer particles in the ferrous study compared to the ferric study, but the sizes of the crystalline particles are comparable.

Morphology

The crystal growth morphologies for the three primary crystal products, t-CPPD, m-CPPD, and o-CPPT, were similar in all five studies. As shown in Figure 7a, the crystals in the control Study III had three morphologies. The most common growth morphology was geodes composed of needles radiating from a central point. These geodes were composed of crystals t-CPPD, m-CPPD, and o-CPPT. There were also feathery composites of crystals which were identified in other pure samples as being o-CPPT. The least frequent crystal morphology was poorly shaped rods or broken plates. The primary crystal growth morphology noted for a sample of t-CPPD, m-CPPD, and o-CPPT from Study I was individual needles [13]. As a representative sample, the growth morphology of a sample from Study V is shown in Figure 7b. This sample came from the ferrous doped layer at week 8 and contains t-CPPD, m-CPPD, and o-CPPT. In addition to the crystal morphologies described for the control samples, there were rare occurrences of t-CPPD crystals with growth morphology paralleling that observed in vivo.

Occluded collagen

The amount of collagen, quantitated by hydroxyproline content, occluded into the crystals as they grew in the gelatin matrix is cited in Table 3. The total amount of crystalline material was quantitated by determining the $[Ca^{+2}]$ in the assay solutions. So as to normalize the amount of hydroxyproline per crystalline mass, the amount of hydroxyproline was divided by the $[Ca^{+2}]$ (Table 3). In the two control Studies I and III, there was significant collagen occlusion in the crystals grown at early times, however, there was no detectable collagen occlusion into crystals which grew at later time points after the initial crystals dissolved. The addition of either ferrous or ferric ions did not seem to change the level of collagen occlusion in the early crystals. However, the presence of both ferrous and ferric ions seemed to enhance the occlusion of collagen in the crystals which grew at later time points.

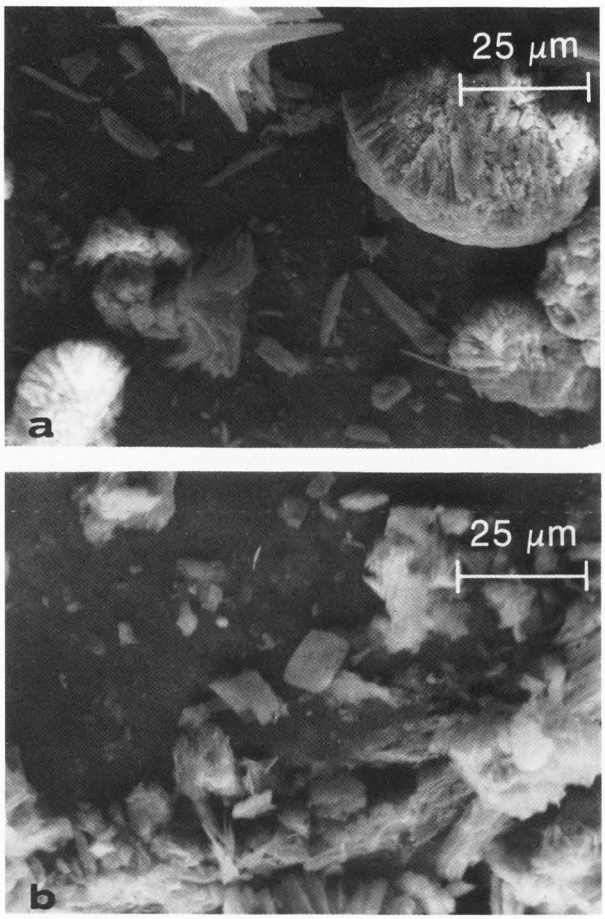

Figure 7: Scanning electron photomicrographs of representative crystalline samples. Figure 7a shows the growth morphologies of crystals t-CPPD, m-CPPD, and o-CPPT in a sample taken from the control Study III at week 18, layer 3. The effect of ferrous ions on the crystal growth morphologies of t-CPPD, m-CPPD, and o-CPPT is shown in Figure 7b using a sample taken from Study V, week 8, layer 4.

Discussion

Previous studies [13,15] have shown that Ca^{+2} and PPi^{-4} ionic diffusion through a denatured collagen matrix at physiologic pH could reproducibly yield the two crystals observed *in vivo* in CPPD crystal deposition disease. This study is part of a series investigating the effect that other ions and crystals, which have been observed coincident with CPPD crystal deposition disease, have on CPPD crystal growth kinetics. The current study focuses on the perturbing effects that ferrous and ferric ions have on CPPD crystal growth kinetics.

Ferric and, to some extent, ferrous ions blocked the progression of the PPi^{-4} diffusion gradient. This retardation in the $[PPi^{-4}]$ gradient led to numerous changes in the kinetics of CPPD crystal formation. At the initial stages of crystal growth, the iron ions induced more crystal growth

Table 3: Hydroxyproline content of selected crystalline samples. Crystals were dissolved, hydroxyproline concentrations determined on the entire sample, and then the calcium concentrations quantitated in the assay solutions. In order to normalize the amount of hydroxyproline per crystalline mass, the concentration of hydroxyproline (ng/ml) was divided by $[Ca^{+2}]$ (mM).

	Day	Layer	Hydroxyproline ng/ml	Ca^{+2} mM	ng/ml mM	Crystal Type
STUDY I	7	4	880	3.12	282	o
(Control)	56	7	0	1.62	0	tmo
STUDY II	14	4	5640	24.33	232	tm
($FeCl_3$)	56	4 - 5	42	10.83	4	tmo
	56	6	49	6.47	7	o
STUDY III	6	4	429	6.36	67	o
(Control)	125	4	0	7.51	0	tmo
STUDY IV	4	4	248	7	35	o
($FeCl_3$)	97	4	15	3.13	5	tmo
STUDY V	6	4	453	6.50	69	o
($FeCl_2$)	55	3	77	4	19	tmo

compared to control. At later incubation times, the iron ions enhanced crystal growth at the expense of crystal nucleation. The presence of both ferrous and ferric ions resulted in the more rapid formation of t-CPPD and m-CPPD crystals. In solution studies, ferric ions also were found to lower the $[PPi^{-4}]$ concentration which is required for CPPD crystal growth to one quarter that required in the absence of iron [8]. In the denatured collagen matrix, the iron ions also reduced the solubility of the crystalline material in the broad diffuse bands which formed when the Ca^{+2} and PPi^{-4} gradients first met. This finding is consistent with McCarty's study on the clearance of preformed, radiolabeled t-CPPD crystals from rabbit joints [17]. They found that synovial hemosiderosis resulted in a 50% increase in the clearance time of the crystals. McCarty, et.al., hypothesized that the decreased clearance rate of t-CPPD crystals was due to ferrous ion inhibition of one or more intracellular pyrophosphatases. The current study suggests that, in addition to this enzyme inhibition, iron ions may also stabilize CPPD crystals against dissolution.

In this *in vitro* system, the presence of either ferrous or ferric ions increased the amount of collagen (hydroxyproline) occluded in the crystalline precipitates formed at later times. At higher levels of ferric ion, iron is also incorporated into the crystals, particularly t-CPPD and m-CPPD. Finally, the presence of iron ions in this *in vitro* system resulted in the rare observation of the *in vivo* crystal growth morphology of t-CPPD. This observation is totally absent from both control Studies I and III.

The results of this *in vitro* study suggest that in biological grade gelatin, iron ions probably bind to the denatured collagen, PPi^{-4} ions bind to the bound iron, leading to CPPD crystallization. This would account for the blockage of the PPi^{-4} gradient, and the occlusion of both collagen and iron within the crystals. The collagen/iron complex apparently leads to the more rapid formation of t-CPPD and m-CPPD crystals in comparison to controls, and at later time points stabilizes the CPPD crystals against dissolution. A possible extrapolation to the *in vivo* setting is that the presence of iron ions surrounding chondrocytes (which are producing PPi^{-4}) could block PPi^{-4} migration, leading to an increased local $[PPi^{-4}]$, and thereby could create an environment favoring CPPD crystal formation.

Several mechanisms have been proposed to explain the association of hemochromatosis and other iron deposition diseases and CPPD crystal deposition. These include changes in synoviocytes, chondrocytes, and cartilage matrix induced by iron. This study shows that ionic iron alone is sufficient to accelerate CPPD crystallization and to stabilize these crystals once formed. The importance of this finding to *in vivo* mechnisms of CPPD crystallization remains unknown.

Acknowledgments

This research was supported in part by grants from the Veterans Administration (#5455-01P to NSM and #5453-02P to GSM), the National Institutes of Health (AR 34096 to GSM, AM 26062 to PBH), the Kroc Foundation for Medical Research, the Fannie E. Ripple Foundation, the Wisconsin Chapter of the Arthritis Foundation, and the Medical College of Wisconsin. Neil S. Mandel is a recipient of an Associate Research Career Scientist Award from the Veterans Administration.

We thank Debra Carroll, Jay Miller, Mike Buday, Kathleen Renne, Craig Cady, and Christine Kuepfer for their technical assistance.

References

1. Abbott DJ, Gresham GA. (1972). Arthropathy in transfusional siderosis. Br Med **1**, 418-419.
2. Brighton CT, Bigley EC, Smolenski BI. (1970). Iron induced arthritis in immature rabbits. Arthritis Rheum **13**, 849-857.
3. Butkowski, RJ, Noelken ME, Hudson BG. (1982). Estimation of the size of collagenous proteins by electrophoresis and gel chromatography. Methods of Enzymology. LW Cunningham, DW Frederiksen.(Eds.). New York, Academic Press, pp 410-423.
4. Dorfmann H, Solinica J, Di Menza C, de Seze C.

(1969). Les arthropathies des hemochromatoses: Resultats d'une enquete prospective portant sur 54 malades. Sem Hop Paris **45**, 516-523.
5. Dymock IW, Hamilton EBD, Laws JW, Williams R. (1970). Arthropathy of haemochromatosis: Clinical and radiological analysis of 63 patients with iron overload. Ann Rheum Dis **29**, 469-476.
6. Fiske CH, SubbaRow Y. (1925). The colorimetric determination of phosphorous. J Biol **66**, 375-403.
7. Hamilton E, Williams R, Barlow KA, Smith PM. (1968). The arthropathy of idiopathic haemochromatosis. Q J Med **37**, 171-182.
8. Hearn PR, Russell RGG, Elliott JC. (1978). Formation product of calcium pyrophosphate crystals in vivo and the effect of iron salts. Clin Sci Mol Med **54**, 29P.
9. Hiyeda K. (1939). On cause of endemic diseases prevailing in Manchoukuo (Kaschin-Beck's disease, so called Kokasan disease, endemic goiter) Trans Soc Pathol Jpn **29**, 325-331.
10. Jensen PS, Putman CE. (1977). Chondrocalcinosis and haemophilia. Clin Rad **28**, 401-405.
11. Lehr J, Brown EH, Frazier AW, Smith JP, Thrasher RD. (1967). Crystallographic properties of fertilizer compounds. Chem Eng Bull TVA **6**, 1-166.
12. Leonello PP, Cleland LG, Norman JE. (1981). Acute pseudogout and chondrocalcinosis in a man with mild hemophilia. J Rheum **8**, 841-844.
13. Mandel NS, Mandel GS. (1984). A model for human calcium pyrophosphate crystal deposition disease: Crystallization kinetics in a gelatin matrix. Scanning Electron Microsc.1984; **IV**, 1779-1793.
14. Mandel N, Mandel G. (1984). Nucleation and growth of CPPD crystals and related species in vitro. Calcium in Biological Systems. RP Reuben, G Weiss, JW Putney.(Eds.). New York, Plenum Press, pp 711-717.
15. Mandel NS, Mandel GS, Carroll DJ, Halverson PB. (1984). Calcium pyrophosphate crystal deposition: An in vitro study using a gelatin matrix model. Arthritis Rheum **27**, 179-186.
16. McCarty DJ, Pepe PF. (1972). Erythrocyte neutral inorganic pyrophosphate in pseudogout. J Lab Clin Med **79**, 277-284.
17. McCarty DJ, Palmer DW, Garancis JC. (1981). Clearance of calcium pyrophosphate dihydrate crystals in vivo: III. Effects of synovial hemosiderosis. Arthritis Rheum **24**, 706-710.
18. Ryan LM, McCarty DJ. (1985). Calcium pyrophosphate crystal deposition disease; Pseudogout; Articular chondrocalcinosis. Arthritis and Allied Conditions. DJ McCarty.(Ed.). Philadelphia, Lea & Febiger,, pp 1515-1546.
19. Schumacher HR. (1972). Ultrastructural characteristics of the synovial membrane in idiopathic haemochromatosis. Ann Rheum Dis **31**, 465-473.
20. Schumacher HR. (1982). Articular cartilage in the degenerative arthropathy of hemochromatosis. Arthritis Rheum **25**, 1460-1468.
21. Schumacher HR. (1985). Ochronosis, hemochromatosis, and Wilson's disease. Arthritis and Allied Conditions. DJ McCarty.(Ed.). Philadelphia, Lea & Febiger, pp 1565-1578.
22. Sella EJ, Goodman AH. (1973). Arthropathy secondary to transfusion hemochromatosis. J Bone Joint Surg **55**, 1077-1081.
23. Stegemann H, Stadler . (1967). Determination of hydroxyproline. Clin Chem Acta **18**, 267-273.

Discussion with Reviewers

R.Z. LeGeros: What is the level of ferrous and ferric ions in diseased states in biological systems?
Authors: In idiopathic hemochromatosis, iron levels have been determined to be 0.019 mg/gm wet weight in synovium and 0.006 mg/gm wet weight in articular cartilage. Comparable data for control patients are 0.013 mg/gm and 0.004 mg/gm, respectively (Hamilton, et al. 1968)

R. Terkeltaub: This model system, as the authors acknowledge, does represent merely a model system. Cartilage is comprised not only of collagen, but of course proteogylcans, cells and a number of proteins whose nature is presently under intense evaluation in a number of laboratories. It is intriguing that in the authors model system forms of CPPD crystals are generated which are similar to those deposited *in vivo* in cartilage. What specific information do the authors have on the effect of proteoglycans on CPPD crystal deposition in this model system?
Authors: At the present time, we have not investigated the effect of proteoglycan on CPPD crystal growth in this system. This is clearly a very important and relevant effect which we are planning to investigate in the near future.

R. Tawashi: It is surprising that Fe^{+3} and Fe^{+2} induced more crystal growth. These additives are believed at least to change the rheological characteristics of the gel. The gel permeability is reduced because of the consolidation of the gel. I wonder how the authors can rule out the effect of gel permeability and crystal poisoning by iron in the process of nucleation and growth?
Authors: Comparison of Figures 2 with 1 and 5a and 6a with 4a shows that the calcium ion gradients are not significantly changed by the presence of either Fe^{+2} or Fe^{+3}, suggesting that gel permeability was not altered significantly. The data presented here indicate that ionic iron initially enhanced crystal nucleation and then, at later times, enhanced crystal growth at the expense of crystal nucleation. These observations are not consistent with crystal poisoning by iron.

R.Tawashi: In Figure 7, growth morphology shows very little. Crystals were grown for different periods of time and taken from different layers of the gel.
Authors: We have looked at the crystal growth morphologies of many other layers and chosen to publish these because they were representative of the morphologies which we did see in other times and layers.